Femtosecond stimulated emission pumping: Characterization of the I 2 − ground state

Martin T. Zanni, Alison V. Davis, Christian Frischkorn, Mohammed Elhanine, and Daniel M. Neumark

Citation: The Journal of Chemical Physics **112**, 8847 (2000); doi: 10.1063/1.481499
View online: http://dx.doi.org/10.1063/1.481499
View Table of Contents: http://scitation.aip.org/content/aip/journal/jcp/112/20?ver=pdfcov
Published by the AIP Publishing

Femtosecond stimulated emission pumping: Characterization of the I_2^- ground state

Martin T. Zanni,[a] Alison V. Davis, Christian Frischkorn, Mohammed Elhanine,[b] and Daniel M. Neumark
Department of Chemistry, University of California, Berkeley, California 94720 and Chemical Sciences Division, Lawrence Berkeley National Laboratory, Berkeley, California 94720

(Received 15 December 1999; accepted 2 March 2000)

Femtosecond stimulated emission pumping in combination with femtosecond photoelectron spectroscopy is used to characterize the potential energy function of the $I_2^-(\tilde{X}\,^2\Sigma_u^+)$ ground state up to vibrational energies within 2% of the dissociation limit. The frequency and anharmonicity of this state are measured at a series of vibrational energies up to 0.993 eV by coherently populating a superposition of ground state vibrational levels using femtosecond stimulated emission pumping, and monitoring the resulting wave packet oscillations with femtosecond photoelectron spectroscopy. The dissociative $I_2^-(\tilde{A}'\,^2\Pi_{g,1/2})$ state is used for intermediate population transfer, allowing efficient population transfer to all ground state levels. Using the measured frequencies and anharmonicities, the $\tilde{X}\,^2\Sigma_u^+$ state has been fit to a modified Morse potential with the β-parameter expanded in a Taylor series, and the bond length, well depth, and $v=0-1$ fundamental frequency set equal to our previously determined Morse potential [J. Chem. Phys. **107**, 7613 (1997)]. At high vibrational energies, the modified potential deviates significantly from the previously determined potential. © *2000 American Institute of Physics.* [S0021-9606(00)01720-7]

I. INTRODUCTION

The photodissociation of I_2^- in size selected $I_2^-(CO_2)_n$, $I_2^-(Ar)_n$ clusters[1–9] and bulk polar solvents[10–13] has become a model system for the study of caging, recombination, and vibrational relaxation. In these systems, the strong solvent/solute effects inherent to negatively charged species induce rapid energy transfer that depends sensitively on the shape of the ground and excited state potentials.[14,15] This is especially true for the ground state potential near the dissociation limit where energy transfer is much more rapid than at low vibrational quanta. For instance, Barbara and co-workers[10,12,13] have shown that within 300 fs of photodissociation, the I_2^- chromophore recombines and relaxes to the lower 25% of the ground state potential in liquid water and ethanol. The remaining relaxation occurs over ~2 ps. Hence, interpretation of the data and quantitative theoretical modeling requires accurate excited and ground state potentials to account for the dissociation and vibrational relaxation processes, respectively. We have previously reported ground and excited state potentials based on a series of frequency and time domain negative ion photoelectron spectroscopy (PES) experiments.[16–18] However, the ground state potential was only characterized near the bottom of the well. In this paper, we use femtosecond photoelectron spectroscopy (FPES) in conjunction with stimulated emission pumping (SEP) to characterize the I_2^- ground state potential to within 2% of the dissociation limit.

Our previous report[16] on the ground state of I_2^- relied on conventional, high-resolution photoelectron spectra to determine the equilibrium bond length (3.205 Å) and well depth (1.014 eV) of I_2^-. To determine the $v=0-1$ vibrational frequency, resonance impulsive stimulated Raman scattering (RISRS) was used to create ground state motion near the bottom of the well. The Fourier transform of the oscillations observed in the FPE spectra gave the fundamental frequency with wave number accuracy ($110\pm2\ cm^{-1}$), and from these three parameters, a Morse potential was determined. Our results differed substantially from previous semiempirical[19–21] and *ab initio* determinations[22–25] of the ground state. The *ab initio* potential by Maslen *et al.*[14,15] has been brought into closer agreement with ours by scaling the potential to reproduce our experimental well depth. However, the ground state potential remains largely unknown at energies above the potential minimum.

In order to characterize the potential at higher energies we utilize gas phase, femtosecond SEP to coherently populate vibrational levels to within 2% of the dissociation limit. Our method is an extension of conventional SEP (Refs. 26, 27) in which a narrow band pump laser populates a single vibrational eigenstate in an excited electronic state. A second, dump pulse then transfers population back to the ground state and into eigenstates resonant with the dump frequency. Hence, by scanning the dump laser wavelength and monitoring the fluorescence depletion, for example, the energies of the ground state levels can be measured and an accurate potential determined. In contrast to conventional SEP, our implementation of SEP utilizes femtosecond pump and dump pulses to coherently populate multiple excited and ground state levels of I_2^-, respectively. In this case, the pump pulse

[a]Current address: Department of Chemistry, University of Pennsylvania, Philadelphia, Pennsylvania 19104.
[b]Permanent address: Laboratoire de Photophysique Moléculaire du CNRS, Bâtiment 210, Université Paris Sud, 91405 Orsay, France.

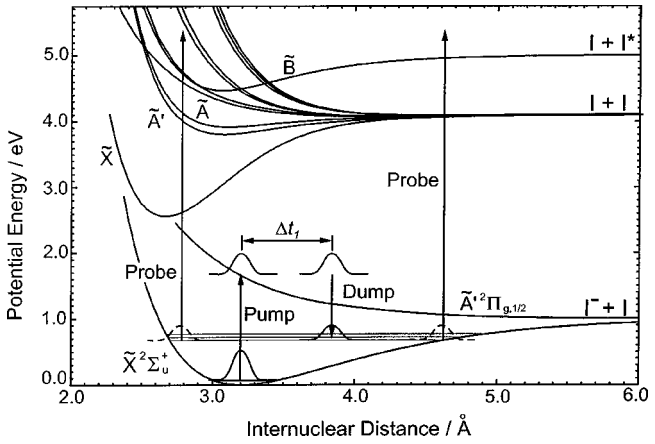

FIG. 1. Schematic of the SEP-FPES technique and relevant I_2^- and I_2 potential energy curves. The SEP process is illustrated using solid curves to represent the excited and ground state wave packets created by the pump and dump pulses, respectively, delayed Δt_1 with respect to each other. Detachment by the probe pulse is shown for two arbitrary delay times, when the ground state wave packet (dashed) is located at the inner and outer turning points.

creates an excited state wave packet for which the Franck–Condon overlap with the ground state vibrational levels constantly evolves with time. With proper timing of the dump pulse, population is coherently transferred back to the ground state, creating a wave packet that oscillates with the frequencies determined by the populated vibrational levels. Hence, by following the wave packet motion in real time, we determine the I_2^- ground state vibrational frequency and anharmonicity as a function of pump and dump wavelengths.

The technique we use to monitor the SEP signal is femtosecond photoelectron spectroscopy (FPES),[17,28] and our approach to create and monitor ground state vibrational motion is illustrated in Fig. 1. In these experiments, a femtosecond pump pulse, centered at ~795 nm, excites I_2^- from its ground $\tilde{X}\,^2\Sigma_u^+$ state to the dissociative $\tilde{A}'\,^2\Pi_{g,1/2}$ potential. After a delay time of 50–150 fs, a second, femtosecond dump pulse transfers a fraction of the evolving excited state wave function back to the ground state and into vibrational levels with energy equal to the difference between the pump and dump laser pulse energies (hereafter referred to as the excitation energy). The vibrationally excited ground state wave packet then oscillates with frequencies characteristic of the energy level spacings that comprise the vibrational distribution. The ensuing dynamics of the depleted $v=0$ ground state, excited state dynamics, and dump induced ground state motion are all monitored by photodetachment with a femtosecond probe pulse at a series of delay times resulting in time-dependent photoelectron spectra. The dynamics of the depleted $v=0$ ground state and evolving excited state wave functions have been reported previously.[16,17] In this article we focus on the dynamics induced by the dump pulse (dashed wave packets).

Our technique is similar in some respects to femtosecond four wave mixing (FWM) techniques[29–31] including femtosecond coherent anti-Raman scattering (CARS) (Refs. 32, 33) and two dimensional time delayed femtosecond CARS.[34] In these experiments two resonant laser pulses, similar to the pump and dump pulses used in our experiment, create a population grating in the ground electronic state. Instead of monitoring the ground state motion by photodetachment, a third pulse is resonantly scattered from the oscillating polarization. Such methods are suitable for studying species that can be created with high number densities. The method described here is far more sensitive, and can be used to study size-selected molecular anions, as we demonstrate in this report.

In this paper, we coherently populate vibrational states up to 0.993 eV on the $I_2^-(\tilde{X}\,^2\Sigma_u^+)$ ground state ($D_e = 1.014$ eV) and use FPES to monitor the resulting oscillatory motion. In this manner, we determine the potential frequency and anharmonicity as a function of vibrational energy, and by modeling our results at successively higher vibrational energies, we have developed a quantitative ground state potential. We also demonstrate that the use of the dissociative $I_2^-(\tilde{A}'\,^2\Pi_{g,1/2})$ electronic state for intermediate population transfer allows for efficient pumping to all ground state levels.

II. EXPERIMENT

The FPES negative ion photoelectron spectrometer and high-repetition rate femtosecond laser have been described in detail elsewhere.[17,35] A brief summary follows, highlighting the modifications made to incorporate an addition dump pulse.

The photoelectron spectrometer consists of an ion source region, time-of-flight (TOF) mass spectrometer, and a high collection efficiency TOF photoelectron spectrometer. I_2^- is produced when argon carrier gas (10 psig) is passed over crystalline iodine, supersonically expanded into the source chamber through a pulsed nozzle operating at 500 Hz, and crossed with a 1 keV electron beam. The I_2^- is isolated from the other anions and clusters formed in the expansion by injection into a Wiley–McLaren TOF mass spectrometer[36] using pulsed extraction and acceleration fields perpendicular to the molecular beam apparatus. After passing through several differentially pumped chambers, the ions enter the photoelectron spectrometer and interact with the pump, dump, and probe laser pulses. The detached electrons are collected with high efficiency using a magnetic bottle,[37] and the 500 Hz repetition rate allows for rapid data collection. Although we often decelerate the ions prior to detachment to improve the photoelectron energy resolution,[17,38,39] in these experiments this is not necessary; as a result the resolution is ~300 meV at 1.7 eV electron kinetic energy (eKE) and degrades approximately as $(\mathrm{eKE})^{1/2}$.

The pump, dump, and probe pulses are obtained from the fundamental of a Clark-MXR regeneratively amplified Ti:sapphire laser system that generates pulses at ~795 nm (1.56 eV) with 1 mJ of energy and 80 fs (sech^2) width. About 40 μJ of this is used as the pump pulse and 500 μJ is used to pump a Light Conversion optical parametric amplifier (OPA) that generates infrared dump pulses from 950 to 2150 nm with an average of 40 μJ energy and 80 fs width. The remaining fundamental is frequency tripled to make 265 nm (4.68 eV), 20 μJ, and 130 fs probe pulses. In order to determine the exact excitation energy, the bandwidths of the

pump and dump pulses are measured with a monochromator prior to each experiment. The relative timing between the three pulses is controlled by two translation stages, and the beams are collinearly recombined prior to entering the vacuum chamber. Because the entrance window affects the timing between the three pulses, above threshold detachment of I^- is used to determine the absolute zero-of-time inside the spectrometer; when any two pulses are temporally overlapped in the chamber, additional peaks are observed for which the time-dependent intensity gives the cross-correlation of the respective pulses.[28,40]

Two procedures were used to normalize the spectra of different pump–dump–probe delay times. When the SEP signal is large, a phase-locked chopper is used to perform shot-to-shot background subtraction by alternately collecting signal with and without the dump pulse to create a difference spectrum. The total background signal is also recorded (pump–probe only), which is constant after 300 fs since the excited state dynamics are complete, and thus can be used to normalize the difference spectra. When the signal is low, as it is for dump frequencies near 1067 nm due to low OPA conversion efficiency, shot-to-shot background is inefficient because the data collection rate is effectively halved. In this case, all spectra are collected with the dump pulse active, and the spectra are normalized by their integrated intensities at each delay time. This is a reliable normalization method because the SEP signal is less than 10% of the total intensity. Although shot-to-shot background subtraction is preferable, the pump–probe background spectra can be subtracted at a later time.

III. RESULTS

Figure 2(a) presents femtosecond photoelectron spectra of I_2^- taken with the probe only (solid), pump and probe (dashed), and pump, dump, and probe pulses active (dotted). The dump wavelength in this figure is 1450 nm (0.86 eV), the pump–dump delay time, Δt_1, is 150 fs, and the pump–probe delay time, Δt_2, is 2200 fs. These spectra have not been background subtracted. In the probe only spectra, peaks are observed at 0.3, 0.9, and 1.45 eV (labeled *B*, *A*, and *X*), primarily due to detachment to the $\tilde{B}\,^3\Pi_{0^+u}$, $\tilde{A}\,^3\Pi_{1u}$ and $\tilde{A}'\,^3\Pi_{2u}$, and $\tilde{X}\,^1\Sigma_g^+$ states of I_2, respectively.[16,41] With inclusion of the pump pulse, a portion of the $v=0$ ground state population is transferred to the $\tilde{A}'\,^2\Pi_{g,1/2}$ excited state, resulting in a bleach of the probe-only spectra that is typically 40%. Additional peaks at 0.75 and 1.70 eV also appear due to detachment of the I^- products to the $I^*(^2P_{1/2})$ and $I(^2P_{3/2})$ spin–orbit states, respectively. Dissociation of I_2^- in this manner takes on the order of 250 fs,[17,28] and in the spectra of Fig. 2(a) this process is already complete. With the addition of the dump pulse (dotted), the atomic I^- features decrease about 10% in intensity due to the transfer of population back to the ground state. However, the probe only features do not increase in intensity. Rather, intensity appears between the I^- features at 1.1 eV as well as at high eKE up to ~3.1 eV. In general, the longer the dump wavelength, the higher in energy the intensity extends. These features are due to photodetachment from high vibrational levels of I_2^-.[6,8]

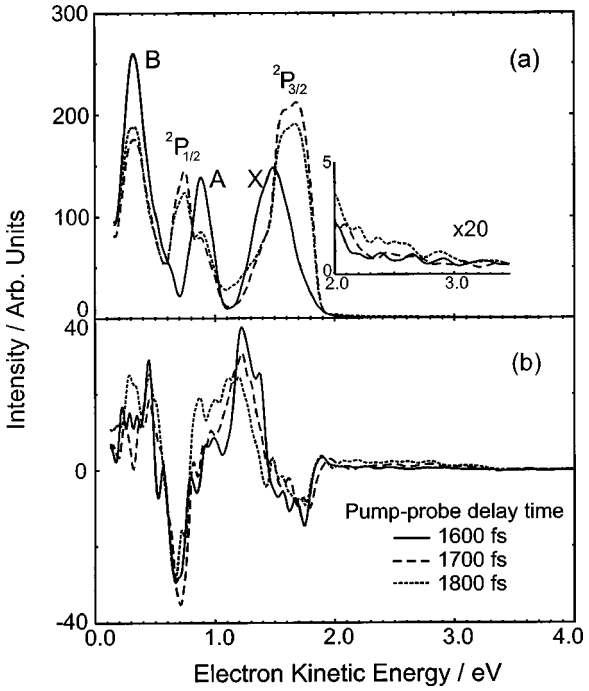

FIG. 2. (a) FPE spectra using solely the probe (solid), pump and probe (dashed), and pump, dump, and probe pulses (dotted), with a dump wavelength of 1450 nm. (b) Spectra taken with shot-to-shot background subtraction active (Sec. II) at three pump–probe delay times.

The pump and dump efficiencies can be determined by comparison of the ground and excited state bleach, respectively, to give an overall efficiency for population transfer to high vibrational levels of the ground state. From the bleach of the probe only spectra, 42% of the ground state population is transferred to the excited state. With addition of the dump pulse, 10% of the excited state wave packet is transferred back to the ground state, as determined from the bleach of the I^- product. Hence, we achieve 4%–5% SEP efficiency. This efficiency is typical for all dump wavelengths used in this report, even for vibrational levels very close to the I_2^- dissociation limit, and is a consequence of using a repulsive state as the intermediate electronic level in the SEP scheme. This point is explored in more detail elsewhere.[42]

Features induced by the dump pulse are more apparent in the shot-to-shot background subtracted mode (Sec. II), as shown in Fig. 2(b). The depletion of the I^- features now show up as negative peaks, and the intensity due to detachment of the vibrationally excited levels is easily observable. At most eKEs, the photoelectron spectrum is rather complex. Between 0.8 and 1.4 eV the photoelectron spectra [Fig. 2(b)] arise from detachment at both the outer and inner turning points of the I_2^- ground state potential, and include detachment to at least 10 energetically accessible I_2 potentials.[17,43] However, the signal extending to high eKE (>2.0 eV) is only due to detachment to the I_2 $\tilde{X}\,^1\Sigma_g^+$ state at the inner turning point of the I_2^- vibrational distribution (Fig. 1).[43] This region of the photoelectron spectrum has previously been used to determine the vibrational distribution of I_2^- products

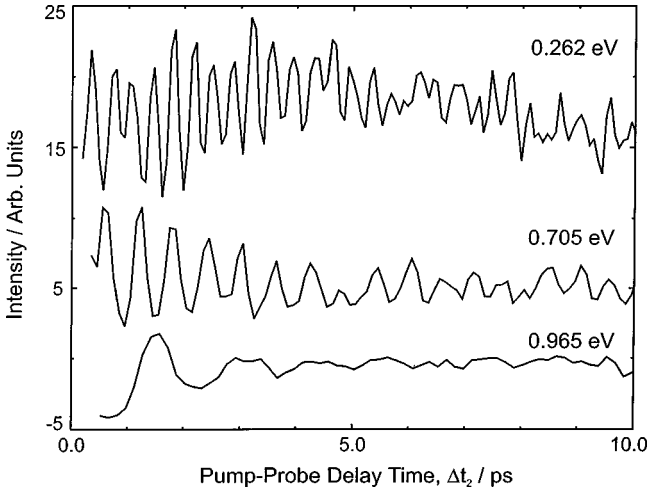

FIG. 3. Slices through the SEP signal for three typical excitation energies. The period of the oscillations increase with excitation energy, and dephasing occurs by ~8 ps.

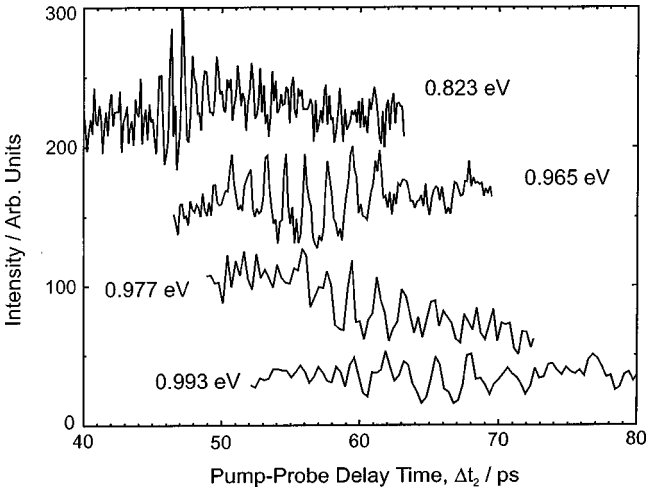

FIG. 4. Recurrences of the four highest excitation energies. The recurrences appear at increasingly longer delay times, indicating the potential's anharmonicity is decreasing with excitation energy.

in photodissociation and cluster recombination experiments.[6,8]

All of these features exhibit oscillatory time-dependent dynamics. For example, above 2.0 eV and at 1.1 eV the signal clearly increases between 1600 and 1800 fs, while a corresponding decrease in intensity is observed at 1.4 eV eKE [Fig. 2(b)]. As established above, the signal above 2.0 eV monitors the ground state population near the inner turning point. Hence, the time-evolution of the spectra in Fig. 2(b) indicates that the ground state wave packet is moving towards the inner turning point during this 200 fs time interval. Since the oscillations at 1.1 and 2.0 eV have similar phases, the inner turning point is also monitored at 1.1 eV, albeit by detachment to I_2 states other than the ground state. On the other hand, the oscillations at 1.4 eV must reflect wave packet motion at the outer turning point, since they are 180° out-of-phase with those at 2.0 eV. In principle the wave packet can be monitored at all internuclear distances. However, the large number of neutral states that contribute to the signal below 2.0 eV make quantitative analysis of the spectra difficult. Hence, in this report, we focus on the portion of the signal above 2.0 eV eKE as this solely monitors wave packet motion near the inner turning point.

The frequency of the oscillations decreases with increasing excitation energy. This is apparent in Fig. 3, where slices through the intensity above 2.0 eV are shown as function of delay time for three different excitation energies, 0.262, 0.705, and 0.965 eV. The oscillations have periods of ~350, 650, and 1500 fs, respectively, and all disappear by roughly 8 ps. However, the oscillations reappear for approximately twice the duration between 40 and 70 ps, depending on the excitation energy; the recurrence time is 42 ps at or below 0.676 eV, and becomes increasingly longer for higher excitation energies. This is illustrated in Fig. 4. For the highest excitation energy used in our experiments (0.993 eV), the oscillations appear near 67 ps and have a period of ~2500 fs.

The time delay, Δt_1, between pump and dump pulses also affects the SEP efficiency. To maximize this, the SEP signal above 2.0 eV was monitored while scanning Δt_1 in 25 fs steps. The optimal Δt_1 increased steadily with excitation energy, from 40 fs at 0.262 eV to 170 fs at 0.993 eV. This trend is consistent with our expectation that the optimal transfer point is at the internuclear distance where the dump pulse is in resonance with the energy difference between the ground and excited state potentials.[44] For excitation energies above 0.6 eV, Δt_1 must be at least 100 fs to observe any SEP signal.

IV. ANALYSIS AND DISCUSSION

In this section we develop an $I_2^-(\tilde{X}\,^2\Sigma_u^+)$ potential that is accurate to within our experimental error. To this end, we first determine the frequency and anharmonicity of the potential at a series of excitation energies. We then explain the analytical potential and the procedure for fitting the measured frequencies and anharmonicities. The fit potential is then compared to previous ground state potentials.

A. Determination of frequencies and anharmonicities

The first step in determining an accurate potential is to extract the frequencies and anharmonicities from the experimental results for each excitation energy. An implicit assumption in this analysis is that the vibrational distribution of the ground state wave packet is centered at the excitation energy, a result demonstrated in simulations that are detailed elsewhere.[42] For excitation energies $\leqslant$0.823 eV, Fourier transforms of the oscillations, shown in Fig. 5, are sufficient to determine the frequencies.[16] However, the transforms are obtained from the recurrences rather than the initial oscillations, because they provide more intense and well-defined transforms. This is demonstrated in Fig. 5 for 0.823 eV of excitation energy, where the Fourier transforms of the initial oscillations (dashed) and recurrences (solid) are compared. Both are centered at the same frequency, but the transform of the recurrences is much more prominent, because the time-envelope in which the recurrences rephase and dephase is twice as long as the envelope that only includes the initial dephasing. Thus, the frequencies used in this report are the

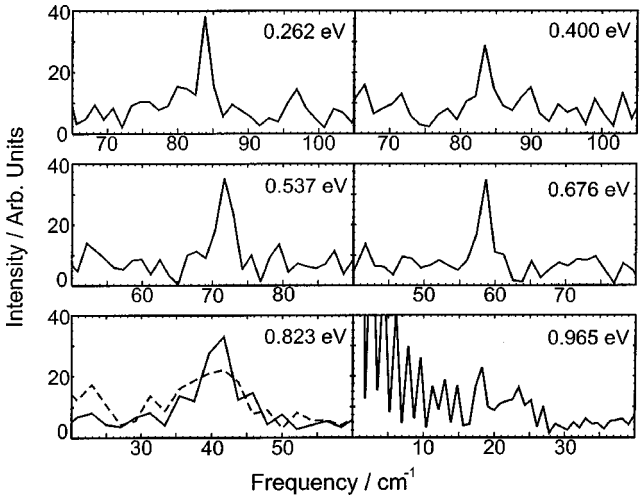

FIG. 5. Fourier transforms of the SEP recurrences used to determine the potential's frequency as a function of excitation energy (Table I). At 0.823 eV, the Fourier transform of the initial oscillations (dashed) is compared to that of the recurrences (solid). At 0.965 eV, the low frequency noise is apparent below 20 cm^{-1}.

Fourier transforms in Fig. 5, which are listed in Table I with the error bars estimated as the FWHM of the transforms.

For excitation energies $\geqslant$0.965 eV, the Fourier transforms become less reliable for two reasons. First, even though the SEP efficiency is similar for all excitation energies, the signal to noise ratio decreases with excitation energy, because the photoelectron spectra are spread out over an increasingly larger range of eKEs (Sec. III). Second, the wave packet frequencies begin to merge with low frequency noise present in our experiments below 20 cm^{-1}, primarily caused by long-term drift in our laser beams. At 0.965 eV, the wave packet frequency can still be extracted from the transform by comparison with transforms lacking the ground state oscillations, but above 0.965 eV this is no longer the case. Nonetheless, the predominant frequency was still estimated from the spectra in Fig. 4 using a least-squares fitting routine in which three sine waves of adjustable frequencies and intensities were fit to each of the rephased oscillations. The average of the three frequencies is listed in Table I. The accuracy of this method was tested for excitation energies of 0.823 and 0.965 eV, which compare reasonably well with the Fourier transforms. Generous error bars are assigned to the frequencies $\geqslant$0.965 eV to account for their semiquantitative nature.

TABLE I. Experiment and fit frequencies and anharmonicities.

Excitation energy/eV	Experimental data		Fit potential	
	Freq/cm^{-1}	Anharm/cm^{-1}	Freq/cm^{-1}	Anharm/cm^{-1}
0.014[a]	110±2		109.9	
2.262	94±1		93.3	
0.400	83.5±1		83.6	
0.537	72±1.5		72.7	
0.676	58±1		59.1	
0.823	41±2.5	0.354±0.016	42.7	0.345
0.965	22±4	0.296±0.015	19.0	0.292
0.977	17±4	0.278±0.014	15.6	0.277
0.993	13±4	0.249±0.011	10.8	0.249

[a]Taken from Ref. 16.

Even though the frequency of the oscillations becomes harder to determine with excitation energy, the anharmonicity can still be accurately established, because it is inversely proportional to the rephasing time. That is, the rephasing time, τ, is determined by the change in frequency between any three adjacent vibrational levels, i.e., $\tau^{-1}=\Delta\omega=\omega_{v+1}-\omega_v$.[43] For a Morse potential, $\Delta\omega=2\omega_e\chi_e$ for any three adjacent vibrational levels. In this case, rephasing will occur at the same time for all excitation energies. For the previously determined $I_2^-(\tilde{X}\,^2\Sigma_u^+)$ Morse potential, the anharmonicity is $\omega e\chi e=0.37\,cm^{-1}$, which gives a rephasing time of $\tau=(2\omega_e\chi_e)^{-1}=45$ ps.[16,45] In our experiment, the rephasing times $\geqslant$0.823 eV become longer with excitation energy (Fig. 4). Hence, the anharmonicity decreases with excitation energy, which indicates deviation from a Morse potential. For the four highest excitation energies, the anharmonicity is determined from the center of the rephasing time and error bars assigned that encompass the edges of the recurrences. The results are listed in Table I.

Very recently, Lineberger and co-workers[46] have measured coherences from highly excited IBr^- formed from photodissociation of IBr_2^-. No rephasing was observed in their experiments, and this was attributed to the variation of the rephasing time with vibrational energy as the dissociation limit of the IBr^- is approached, combined with a broad vibrational energy distribution for the IBr^- product ($\sim$0.5 eV). In our experiment, the I_2^- vibrational distribution is considerably narrower, since it is determined by the convoluted linewidths of the pump and dump pulses ($\sim$0.02 eV), so the variation of rephasing time is actually observed rather than being averaged out.

B. I_2^- ground state potential

In the previous section we determined the vibrational frequencies and anharmonicities for excitation energies up to 0.993 eV. In this section, an I_2^- ground state is constructed by an iterative fit to the data points (Table I). This is done using a Morse potential with the β-parameter expanded in a Taylor series, and with the bond length held constant,[47]

$$V(r)=D_e[1-e^{-\beta(r-r_e)}]^2, \tag{1}$$

$$\beta=\beta_0+\beta_1(r-r_e)+\beta_2(r-r_e)^2+\cdots, \tag{2}$$

where D_e and r_e are the previously determined well depth (1.014 eV) and equilibrium internuclear distance (3.205 Å), respectively.[16] Equations (1) and (2) allow sufficient flexibility to adequately fit the data, but only require the equilibrium internuclear distance. Up to an eighth order expansion of the β-parameter was used [Eq. (2)], although it was found going beyond fourth order did not significantly improve the fit.

Our procedure for determining the potential is as follows. First, a reasonable potential is generated with an appropriate choice of β-parameters using Eqs. (1) and (2). The vibrational eigenstates are then calculated using a discrete variable representation (DVR) code with a Morse oscillator basis set,[48] and the frequency and anharmonicity are deter-

TABLE II. β-parameters for the fit potential.

$\beta_0 = 1.88\,497\ \text{Å}^{-1}$	$\beta_1 = -6.810\,537\times10^{-2}\ \text{Å}^{-2}$
$\beta_2 = 1.305\,919\times10^{-2}\ \text{Å}^{-3}$	$\beta_3 = -2.957\,611\times10^{-3}\ \text{Å}^{-4}$
$\beta_4 = 1.941\,355\times10^{-4}\ \text{Å}^{-5}$	

mined for each excitation energy. A statistical analysis is performed with the calculated values and experimental data (Table I), and χ^2 is determined. The method is then repeated with different β-parameters. The entire procedure is automated using a downhill simplex method to iteratively improve the β-parameters and minimize χ^2.[49] Nonlinear least squares fitting was not used because of the difficulty in determining the first derivative of the fitted points with respect to the β-parameters. The parameters of the fit potential are listed in Table II, and the fit frequencies and anharmonicities are compared to experiment in Table I and in Figs. 6 and 7. The agreement is remarkably good; all the calculated frequencies and anharmonicities fall within the experimental error bars. The potential itself is shown in Fig. 8.

It should be noted that rotational dynamics have not been included in the above calculations and discussion, even though Gruebele *et al.*[50,51] have shown that modeling the time-dependent rotational and vibrational wave packet dynamics is equivalent to determining the potential using a RKR inversion technique with frequency resolved eigenstates. The angular distribution of the detached electrons does rotate with the molecular frame, but we are insensitive to this variation because we collect nearly all the photoelectrons in our apparatus. Also, in contrast to absorption experiments, the photodetachment probability is independent of molecular orientation.[52] Hence, we cannot monitor rotational dynamics, which limits our choices for analytical potentials to forms that have energy independent bond lengths.

C. Comparison with other potentials

In this section we compare our potential to the previous Morse[16] and scaled *ab initio* potentials developed by Parson and co-workers.[14,15] For the Morse potential, the vibrational frequency and anharmonicities of the potential at the measured excitation energies were determined using the DVR code described above, and the results are compared to the values from experiment and our fit potential in Figs. 6 and 7. The potentials are shown in Fig. 8. The vibrational frequencies from the Morse potential agree with the fit potential until 0.2–0.3 eV, above which the Morse potential frequencies are noticeably larger. In addition, above 0.8 eV, the (constant) anharmonicity of the Morse potential becomes significantly larger than the fit and experimental anharmonicities. The combination of these effects indicates that the attractive branch of the Morse potential is too steep at high energy, as can be seen more explicitly by comparing the fit and Morse potentials in Fig. 8. Overall, the Morse potential is a good approximation below ~0.3 eV. Interestingly, Morse potentials are overly attractive at large internuclear distances for neutral molecules,[53] but for I_2^- the Morse po-

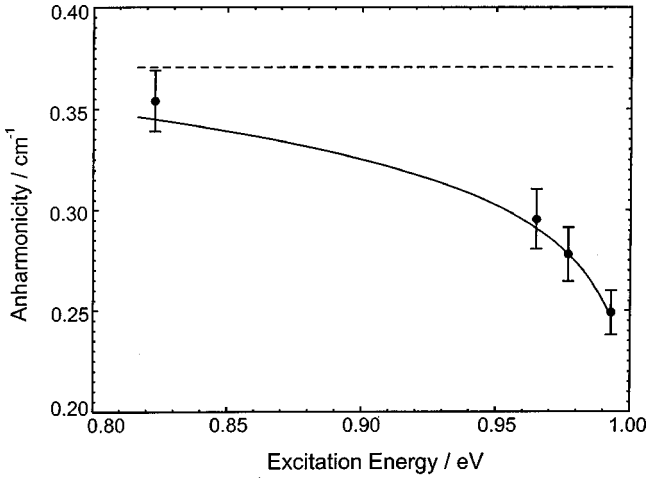

FIG. 7. Comparison of the experimental anharmonicities (circles) to those of the fit potential (solid) and previously determined Morse potential (dashed, Ref. 16).

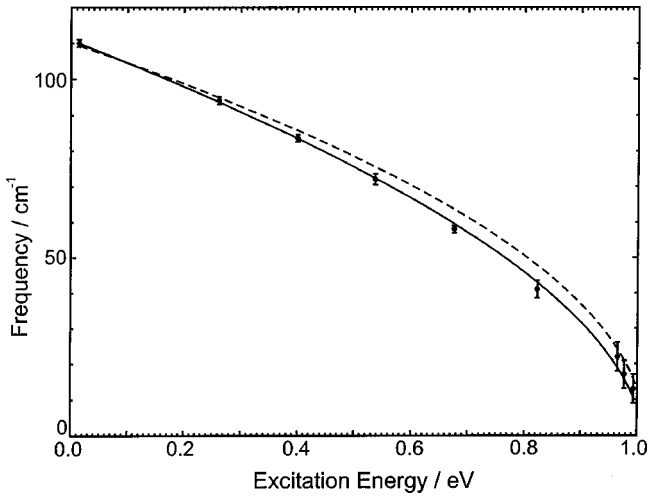

FIG. 6. Comparison of experimental frequencies (circles) to those of the fit potential (solid) and previously determined Morse potential (dashed, Ref. 16).

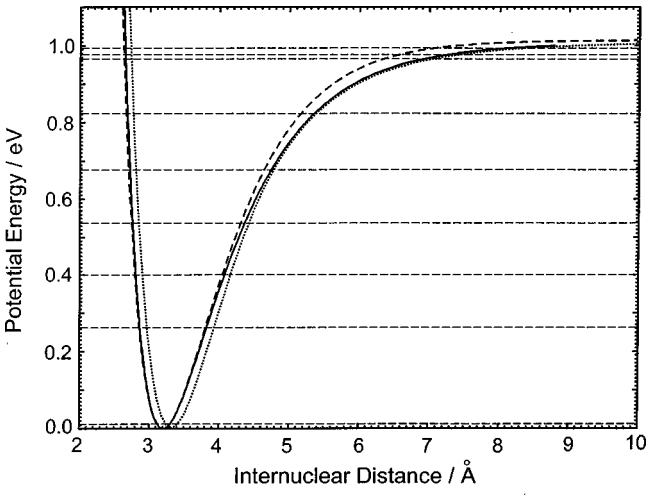

FIG. 8. Comparison of the fit potential (solid) to the previously determined Morse potential (dashed, Ref. 16) and scaled *ab initio* potential (dotted, Refs. 14, 15). The horizontal dotted lines are the excitation energies used to determine the fit potential (Table I).

tential is not sufficiently attractive when compared to our potential. This is likely to be the effect of the $1/r^4$ charge-induced dipole potential inherent to negative ion systems (vs $1/r^6$ for neutrals).

Comparison with the scaled *ab initio* potential shows the opposite trend. In Fig. 8, the *ab initio* potential agrees well with ours for energies above 0.7 eV and internuclear distances greater than 4.5 Å. At smaller radii the potential deviates from ours, primarily because the calculated equilibrium nuclear distance is too large. The agreement between our empirical potential and the scaled *ab initio* potential for radii above 4.5 Å is consistent with our work on the $I_2^-(\tilde{A}'\,^2\Pi_{g,1/2})$ excited state surface where similar agreement at large internuclear distances was found.[17] This agreement indicates that the *ab initio* methods are reliable at calculating potentials for large radii. It also strengthens the conclusions drawn from theoretical calculations studying the recombination and vibrational relaxation rates of photodissociated $I_2^-(Ar)_n$ and $I_2^-(CO_2)_n$ clusters,[14,15,54–56] since the *ab initio* potentials are very accurate at large internuclear distances where these processes are exceedingly sensitive to the potential surfaces. We note that a new *ab initio* potential by Vala and co-workers[57] produces better agreement with our potential closer to the equilibrium distance.

V. CONCLUSION

In this report we have applied femtosecond stimulated emission pumping to anions for the first time. By monitoring the resulting ground state wave packet with FPES, we have demonstrated its utility in accessing a wide range of vibrational levels to allow the determination of an accurate ground state potential. Specifically, we measured the frequency and anharmonicity of the I_2^- ground state to within 2% of the dissociation limit and fit the results to a Morse potential with a β-parameter expanded in a Taylor series. Our results yield a potential that is significantly more attractive than the previousl determined Morse potential at high vibrational energies. It was also shown that the use of a dissociative state for intermediate population transfer allows a wide range of ground state vibrational energies to be accessed.

ACKNOWLEDGMENTS

D.M.N. acknowledges support from the National Science Foundation under Grant No. CHE-9710243 and from the Defense University Research Instrumentation Program under Grant No. F49620-95-0078. C.F. acknowledges postdoctoral support from the Deutsche Akademie der Naturforscher Leopoldina (BMBF-LPD 9801-6). A.V.D. is a National Science Foundation predoctoral fellow. The authors would also like to thank Steve Leone and David Tannor for helpful discussions, and Iddo Pinkas for a copy of Ref. 34 prior to publication.

[1] J. M. Papanikolas, J. R. Gord, N. E. Levinger, D. Ray, V. Vorsa, and W. C. Lineberger, J. Phys. Chem. **95**, 8028 (1991).
[2] J. M. Papanikolas, V. Vorsa, M. E. Nadal, P. J. Campagnola, H. K. Buchenau, and W. C. Lineberger, J. Chem. Phys. **99**, 8733 (1993).
[3] V. Vorsa, S. Nandi, P. J. Campagnola, M. Larsson, and W. C. Lineberger, J. Chem. Phys. **106**, 1402 (1997).
[4] A. Sanov, S. Nandi, and W. C. Lineberger, J. Chem. Phys. **108**, 5155 (1998).
[5] A. Sanov, T. Sanford, S. Nandi, and W. C. Lineberger, J. Chem. Phys. **111**, 664 (1999).
[6] B. J. Greenblatt, M. T. Zanni, and D. M. Neumark, Science **276**, 1675 (1997).
[7] M. T. Zanni, B. J. Greenblatt, and D. M. Neumark, J. Chem. Phys. **109**, 9648 (1998).
[8] B. J. Greenblatt, M. T. Zanni, and D. M. Neumark, J. Chem. Phys. **111**, 10566 (1999).
[9] B. J. Greenblatt, M. T. Zanni, and D. M. Neumark, J. Chem. Phys. **112**, 601 (2000).
[10] A. E. Johnson, N. E. Levinger, and P. F. Barbara, J. Phys. Chem. **96**, 7841 (1992).
[11] J. C. Alfano, Y. Kimura, P. K. Walhout, and P. F. Barbara, Chem. Phys. **175**, 147 (1993).
[12] I. Benjamin, P. F. Barbara, B. J. Gertner, and J. T. Hynes, J. Phys. Chem. **99**, 7557 (1995).
[13] P. K. Walhout, J. C. Alfano, K. A. M. Thakur, and P. F. Barbara, J. Phys. Chem. **99**, 7568 (1995).
[14] J. Faeder, N. Delaney, P. E. Maslen, and R. Parson, Chem. Phys. Lett. **270**, 196 (1997).
[15] J. Faeder, N. Delaney, P. E. Maslen, and R. Parson, Chem. Phys. **239**, 525 (1998).
[16] M. T. Zanni, T. R. Taylor, B. J. Greenblatt, B. Soep, and D. M. Neumark, J. Chem. Phys. **107**, 7613 (1997).
[17] M. T. Zanni, V. S. Batista, B. J. Greenblatt, W. H. Miller, and D. M. Neumark, J. Chem. Phys. **110**, 3748 (1998).
[18] V. S. Batista, M. T. Zanni, B. J. Greenblatt, D. M. Neumark, and W. H. Miller, J. Chem. Phys. **110**, 3736 (1998).
[19] E. C. M. Chen and W. E. Wentworth, J. Phys. Chem. **89**, 4099 (1985).
[20] J. G. Dojahn, E. C. M. Chen, and W. E. Wentworth, J. Phys. Chem. **100**, 9649 (1996).
[21] E. C. M. Chen, J. G. Dojahn, and W. E. Wentworth, J. Phys. Chem. A **101**, 3088 (1997).
[22] P. W. Tasker, G. G. Balint-Kurti, and R. N. Dixon, Mol. Phys. **32**, 1651 (1976).
[23] G. A. Bowmaker, P. Schwerdfeger, and L. v. Szentpaly, J. Mol. Struct.: THEOCHEM **53**, 87 (1989).
[24] D. Danovich, J. Hrusak, and S. Shaik, Chem. Phys. Lett. **233**, 249 (1995).
[25] P. E. Maslen, J. Faeder, and R. Parson, Chem. Phys. Lett. **263**, 63 (1996).
[26] C. Kittrell, E. Abramson, J. L. Kinsey, S. McDonald, D. E. Reisner, D. Katayama, and R. W. Field, J. Chem. Phys. **75**, 2056 (1981).
[27] M. Drabbels and A. M. Wodtke, J. Phys. Chem. A **103**, 7142 (1999).
[28] B. J. Greenblatt, M. T. Zanni, and D. M. Neumark, Chem. Phys. Lett. **258**, 523 (1996).
[29] M. Motzkus, S. Pedersen, and A. H. Zewail, J. Phys. Chem. **100**, 5620 (1996).
[30] M. Schmitt, G. Knopp, A. Materny, and W. Kiefer, Chem. Phys. Lett. **280**, 339 (1997).
[31] E. J. Brown, Q. Zhang, and M. Dantus, J. Chem. Phys. **110**, 5772 (1999).
[32] C. Hayden and D. W. Chandler, J. Chem. Phys. **103**, 10465 (1995).
[33] M. Schmitt, G. Knopp, A. Materny, and W. Kiefer, Chem. Phys. Lett. **270**, 9 (1997).
[34] G. Knopp, I. Pinkas, and Y. Prior, J. Raman Spectrosc. **31**, 51 (2000).
[35] B. J. Greenblatt, M. T. Zanni, and D. M. Neumark, Faraday Discuss. **108**, 101 (1998).
[36] W. C. Wiley and I. H. McLaren, Rev. Sci. Instrum. **26**, 1150 (1955).
[37] O. Cheshnovsky, S. H. Yang, C. L. Pettiette, M. J. Craycraft, and R. E. Smalley, Rev. Sci. Instrum. **58**, 2131 (1987).
[38] H. Handschuh, G. Gantefor, and W. Eberhardt, Rev. Sci. Instrum. **66**, 3838 (1995).
[39] L.-S. Wang, H.-S. Cheng, and J. Fan, J. Chem. Phys. **102**, 9480 (1995).
[40] M. D. Davidson, B. Broers, H. G. Muller, and H. B. v. L. v. d. Heuvell, J. Phys. B **25**, 3093 (1992).
[41] K. R. Asmis, T. R. Taylor, C. Xu, and D. M. Neumark, J. Chem. Phys. **109**, 4389 (1998).
[42] M. T. Zanni, Ph.D. thesis, University of California, Berkeley, 1999.
[43] M. T. Zanni, B. J. Greenblatt, A. V. Davis, and D. M. Neumark, J. Chem. Phys. **111**, 2991 (1999).
[44] R. S. Mulliken, J. Chem. Phys. **55**, 309 (1971).
[45] M. T. Zanni, B. J. Greenblatt, A. V. Davis, and D. M. Neumark, Proc. SPIE **3271**, 196 (1998).

[46] A. Sanov, T. Sanford, L. J. Butler, J. Vala, R. Kosloff, and W. C. Lineberger, J. Phys. Chem. A **103**, 10244 (1999).
[47] W. N. Whitton and P. J. Kuntz, J. Chem. Phys. **64**, 3624 (1976).
[48] E. M. Greenawalt and A. S. Dickinson, J. Mol. Spectrosc. **30**, 427 (1969).
[49] W. H. Press, B. P. Flannery, S. A. Teukolsky, and W. T. Vetterling, *Numerical Recipes* (Cambridge University Press, Cambridge, 1989).
[50] M. Gruebele, G. Roberts, M. Dantus, R. M. Bowman, and A. H. Zewail, Chem. Phys. Lett. **166**, 459 (1990).
[51] M. Gruebele and A. H. Zewail, J. Chem. Phys. **98**, 883 (1993).
[52] E. P. Wigner, Phys. Rev. **73**, 1002 (1948).
[53] J. I. Steinfeld, J. S. Francisco, and W. L. Hase, *Chemical Kinetics and Dynamics* (Prentice–Hall, New Jersey, 1989).
[54] J. Faeder and R. Parson, J. Chem. Phys. **108**, 3909 (1998).
[55] N. Delaney, J. Faeder, and R. Parson, J. Chem. Phys. **111**, 651 (1999).
[56] N. Delaney, J. Faeder, and R. Parson, J. Chem. Phys. **111**, 452 (1999).
[57] J. Vala, R. Kosloff, and J. Harvey (in preparation).